Electronic Supplementary Material

The mechanochemical excitation of crystalline LiN_3

Adam A.L. Michalchuk

Federal Institute for Materials Research and Testing (BAM), Richard-Wilstaetter Str 11, 12489, Berlin, Germany

S1 COMPRESSIBILITY AND ADIABATIC HEATING

The following section outlines the *ab initio* compressibility of the model crystal systems up to a maximum pressure of 5 GPa, alongside consideration for the effective adiabatic heating that results from this compression. Within our model, the final temperature, T_f obtained from adiatically compressing a solid is obtained according to

$$T_f = T_0\left(\frac{V}{V_0}\right)^{-\Gamma}$$

To calculate the approximate vibrational Gruneisen parameter, the Brillouin zone centre vibrational frequencies were calculated at increasing compression from ambient pressure to 5 GPa.

S1.1 Compression and heating of LiN_3

Table S1.1| Effects of pressure on the unit cell geometry of LiN_3, as obtained from PBE-D2 simulations.

***p*/GPa**	**a=b**	**c**	α	β	γ	**V**
0	3.24260	4.95404	75.75320	104.24680	118.56737	43.83311
1	3.20305	4.87984	76.79810	103.20190	118.51084	42.41172
2	3.17178	4.83397	77.44244	102.55756	118.50815	41.34411
3	3.14435	4.79355	77.98540	102.0146	118.53076	40.39856
4	3.12020	4.75777	78.44599	101.55401	118.56519	39.56202
5	3.09850	4.72616	78.83972	101.16028	118.60373	38.81413
6	3.07885	4.69822	79.17800	100.82200	118.64198	38.14346
7	3.06086	4.67335	79.47376	100.52624	118.68106	37.53566
8	3.04420	4.65060	79.73658	100.26342	118.71679	36.97772
9	3.02875	4.63016	79.96801	100.03199	118.75243	36.46630
10	3.01433	4.61142	80.17716	99.82284	118.78737	35.99319

Table S1.2| Effect of pressure on the principal strain axes in LiN_3 as obtained from PBE-D2 simulations. Note $\chi_1 = -0.5454a + 0.5268b + 0.6519c$; $\chi_2 = 0.7038a + 0.7104b + 0.0002c$; $\chi_3 = -0.5686a + 0.5573b - 0.6051c$

***p*/GPa**	χ_1 **/%**	χ_2 **/%**	χ_3 **/%**
0	0.0	0.0	0.0
1	-2.1764	-1.1379	0.0373
2	-3.6087	-2.0997	-0.0787

3	-4.8457	-2.9792	-0.2213
4	-5.9195	-3.7738	-0.3812
5	-6.8606	-4.4979	-0.5538
6	-7.6900	-5.1577	-0.7335
7	-8.4298	-5.7669	-0.9133
8	-9.1027	-6.3299	-1.0958
9	-9.7096	-6.8550	-1.2765
10	-10.2666	-7.3470	-1.4526

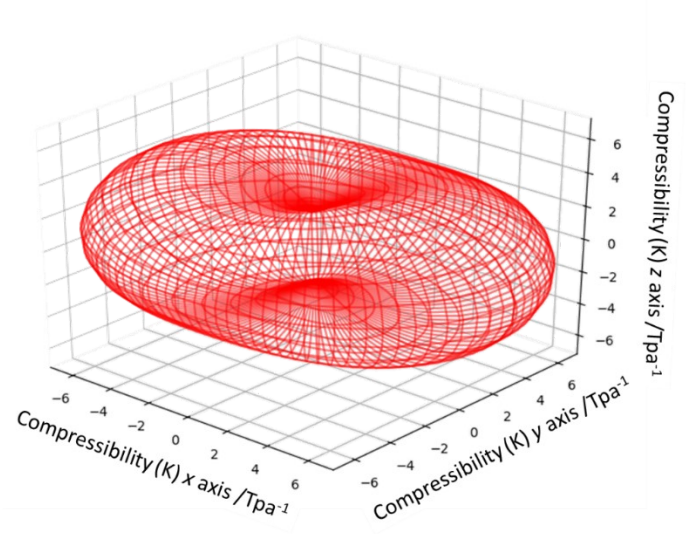

Figure S1.1| Compressibility indicatrix for LiN_3 obtained from PBE-D2 simulation data. Figure prepared from M. J. Cliffe and A. L. Goodwin, *J Appl Crystallogr*, 2012, 45, 1321–1329.

S2 PRESSURE DEPENDENCE OF VIBRATIONAL FREQUENCIES

Table S2.1| Effects of hydrostatic compression on the Brillouin zone centre vibrational frequencies of LiN_3 alongside the mode-dependent Gruneisen parameters, γ.

	Ambient	γ	1 GPa	2 GPa	3 GPa	4 GPa	5 GPa
				Vibrational frequencies /cm^{-1}			
M4	106.55	3.22346	116.69	125.03	133.22	141.27	148.71
M5	154.25	3.47282	173.28	186.51	198.62	209.78	220.00
M6	184.42	3.85726	205.96	224.84	241.92	257.54	271.73
M7	205.90	2.74018	222.41	237.27	250.98	263.44	275.15
M8	300.22	1.62556	313.05	326.89	338.96	349.84	360.12
M9	624.46	-0.09424	622.21	620.82	619.54	618.35	617.24
M10	628.25	-0.11778	625.54	623.77	622.14	620.59	619.17
M11	1369.89	0.15099	1376.32	1381.52	1386.43	1390.98	1395.28
M12	2191.48	0.13756	2200.10	2207.92	2215.28	2222.06	2228.48
						1.5	
	6 GPa		**7 GPa**	**8 GPa**	**9 GPa**	**10 GPa**	
				Vibrational frequencies /cm^{-1}			
M4	155.80 (^{B}g)		162.40 (^{B}g)	168.78 (^{B}g)	174.70 (^{B}u)	180.35 (^{B}u)	
M5	229.32 (^{A}g)		237.93 (^{A}g)	246.01 (^{A}g)	253.47 (^{A}g)	260.51 (^{A}g)	
M6	285.10 (^{A}u)		296.49 (^{B}u)	306.33 (^{B}u)	315.66 (^{B}u)	324.56 (^{B}u)	
M7	286.13 (^{B}u)		297.35 (^{A}u)	309.06 (^{A}u)	319.88 (^{A}u)	330.18 (^{A}u)	
M8	369.87 (^{B}u)		379.16 (^{B}u)	388.39 (^{B}u)	397.20 (^{B}u)	405.78 (^{B}u)	
M9	616.19 (^{A}u)		615.27 (^{A}u)	614.39 (^{A}u)	613.57 (^{A}u)	612.80 (^{A}u)	
M10	617.82 (^{B}u)		616.55 (^{B}u)	615.35 (^{B}u)	614.24 (^{B}u)	613.16 (^{B}u)	
M11	1399.39 (^{A}g)		1403.27 (^{A}g)	1406.98 (^{A}g)	1410.57 (^{A}g)	1414.01 (^{A}g)	
M12	2234.68 (^{B}u)		2240.58 (^{B}u)	2246.21 (^{B}u)	2251.75 (^{B}u)	2257.06 (^{B}u)	

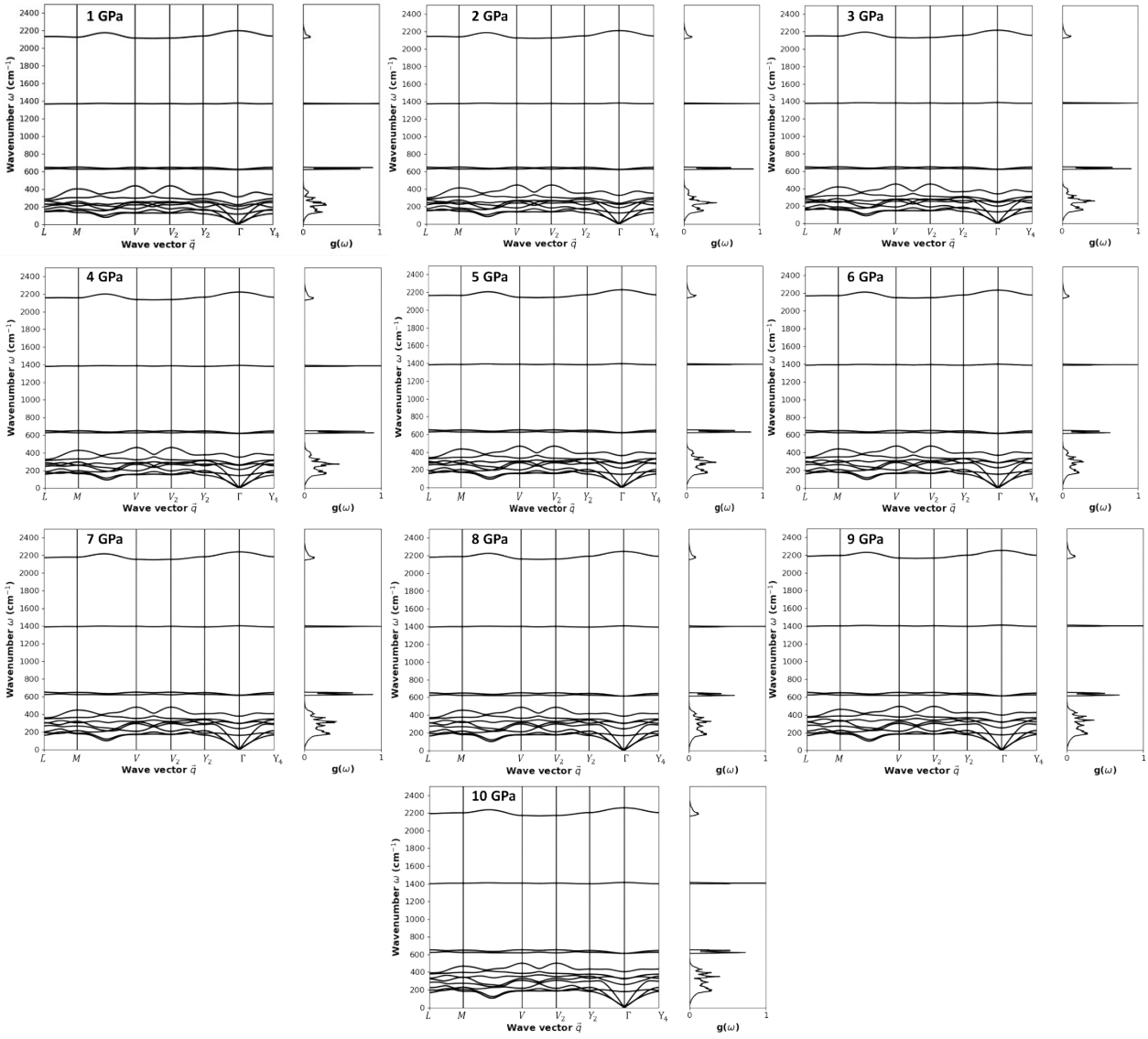

Figure S2.1| Phonon dispersion curves for LiN_3 as a function of hydrostatic compression to 10 GPa. All dispersion curves were generated using a 3 x 3 x 3 supercell and density of states generated by integration over 15 x 15 x 15 *q*-point mesh.

S3 PRESSURE DEPENDENCE OF HEAT CAPACITY

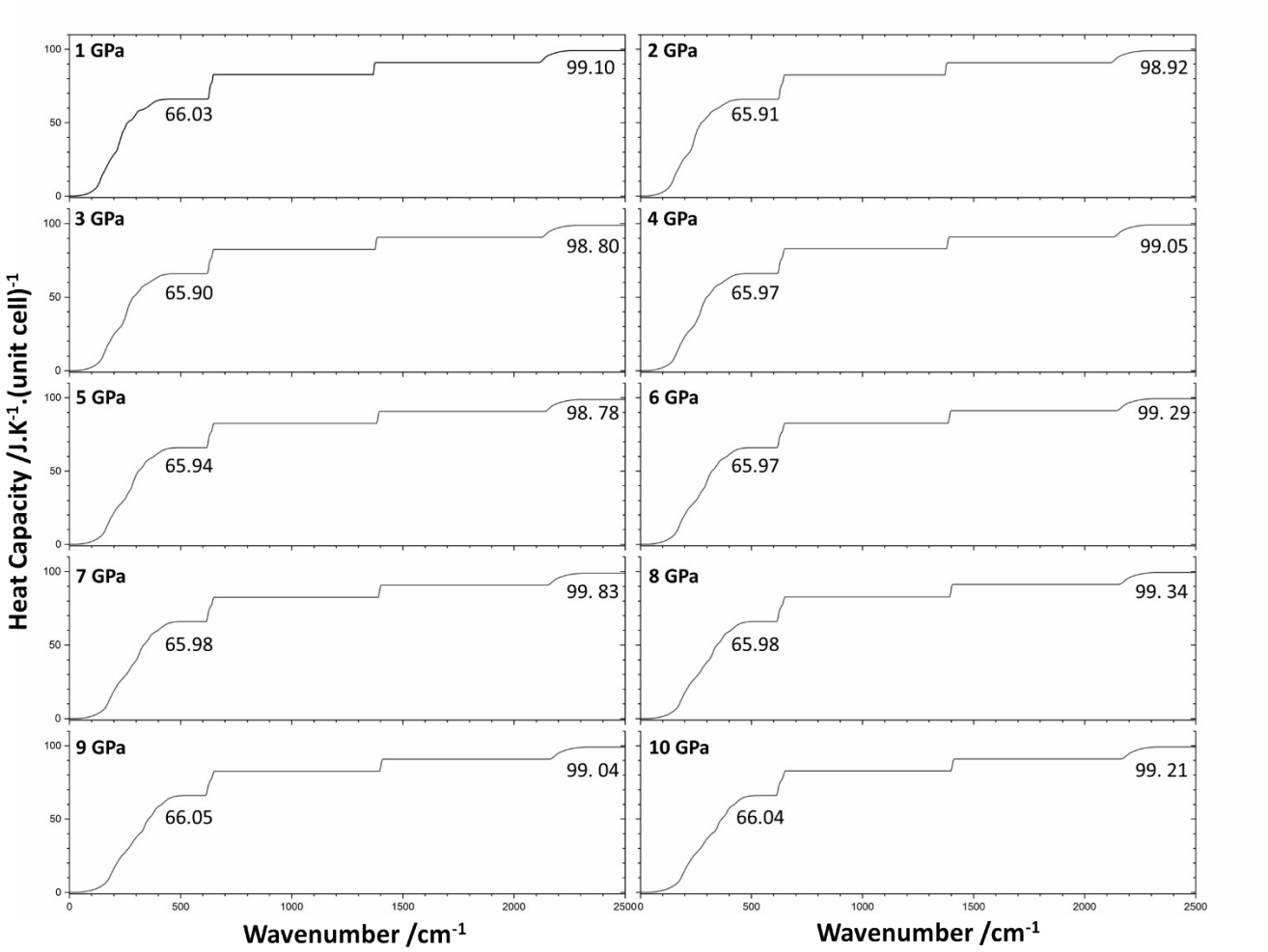

Figure S3.1| Effect of hydrostatic compression on the heat capacity of LiN_3. Values are given for the total and phonon heat capacities.

S4 AB INITIO MOLECULAR DYNAMICS SIMULATIONS

Ab initio molecular dynamics simulations allow for a fully anharmonic description of the material vibrations, and are therefore not restricted to the harmonic approximation. Such calculations therefore provide a reasonable approximation for how a given system will evolve at a given set of thermodynamic conditions. In our simulations we see significant change in the geometry of the N_3^- molecular as a function of time, when at a thermally excited state. At 500 K the bending angle fluctuates around *ca.* 172°, reaching a minimum of 162° over the sampled time period. Instead, at 600 K the bond angle fluctuates around *ca.* 169°, reaching a minimum angle of *ca.* 156°. This is a 24° change in the equilibrium bond angle and is met with > 1eV change in the electronic band gap by comparison with isostructural NaN_3.

It is worth noting that such calculations are certainly a simplification of the excitation observed under dynamic mechanical loading, but do represent a rough idea for the types of distortions that can be expected when the material is excited to these quasi-temperatures.

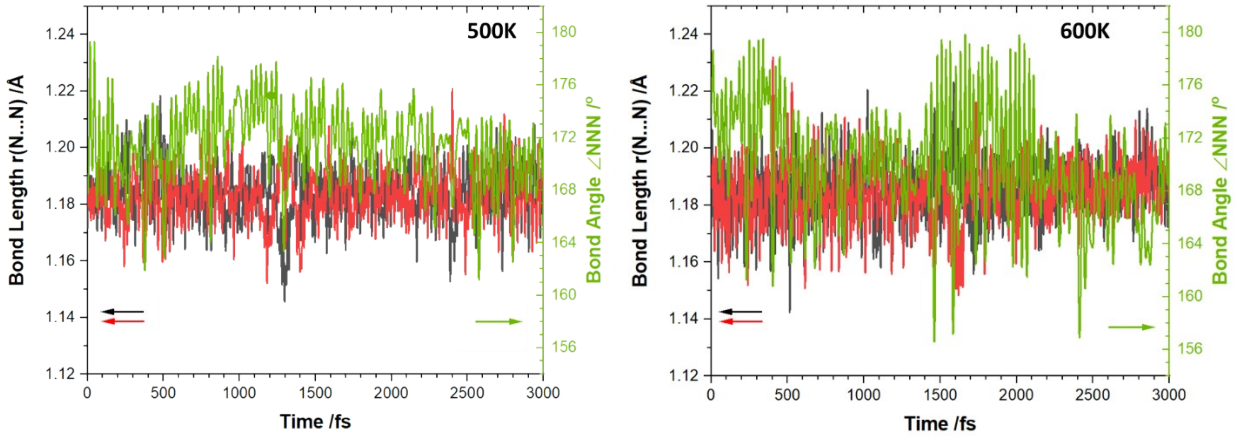

Figure S5.1| Evolution of N_3^- molecule geometry in the LiN_3 crystal unit cell as a function of time at 500 K and 600 K. The angle bend is given in green, and the two N-N bonds are denoted in black and red.

S5 ANISOTROPIC COMPRESSION

The above models make the significant assumption of hydrostatic compression. To gain closer access to the mechanical regime accessed during mechanochemical processing, we consider here the effects of anisotropic compression, restricting discussion to compressions along the direct crystal lattice vectors, and hence omitting any discussion of shear. Although such considerations are likely more representative of mechanochemical conditions, omission of shear is a significant assumption, and its inclusion will be considered in a dedicated follow up investigation.

S5.1 Anisotropic Compression of *a* axis.

To explore uniaxial compression of the *a* axis, the *a* axis was systematically compressed while the remaining unit cell parameters and ion positions were allowed to relax, Table S5.1 To a maximum strain of *ca.* 7% on the *a* axis, the overall volume of the unit cell reduces by *ca.* 4.8% with slight expansion of the crystallographic *b* axis being observed. With compression of the *a* axis, three of the external modes harden, whereas two soften, Table S5.2. This reflects a significant difference in the dynamical response of LiN_3 under hydrostatic and non-hydrostatic loading. Most notable is M7 (comprising a translational motion of both Li and N_3 species), which hardens with a mode Grüneisen parameter of > 8, Table S5.3, although the mode averaged Grüneisen parameter reaches only 1.06, notably smaller than achieved for hydrostatic compression owing to the marked softening of vibrational bands under uniaxial compression.

Table S5.1 Effects of anisotropic compression of *a* axis on the lattice parameters.

a/a_0 /%	**a**	**b**	**c**	α	β	γ	**Vol**
1	3.210	3.245	4.932	76.419	104.142	118.342	43.429
5	3.080	3.255	4.942	76.456	103.125	117.119	42.464
7	3.016	3.268	4.920	77.673	103.869	116.691	41.740

Table S5.2 Effect of anisotropic compression of the *a* axis on the Γ point vibrations of LiN_3

1% Compress.				5% Compress.				7% Compress.			
	ν /cm^{-1}		ν /cm^{-1}		ν /cm^{-1}		ν /cm^{-1}		ν /cm^{-1}		ν /cm^{-1}
M4	109.85	**M9**	622.73	**M4**	110.93	**M9**	623.07	**M4**	120.46	**M9**	615.51
M5	160.57	**M10**	627.66	**M5**	153.03	**M10**	624.82	**M5**	127.19	**M10**	627.43
M6	179.28	**M11**	1371.92	**M6**	166.96	**M11**	1377.15	**M6**	173.50	**M11**	1384.21
M7	214.37	**M12**	2193.85	**M7**	252.97	**M12**	2206.05	**M7**	287.02	**M12**	2213.28
M8	302.13			**M8**	324.81			**M8**	348.34		

Table S5.3 Mode Grüneisen parameters (γ) for uniaxial compression of the *a* axis to a strain of 7%.

	γ		γ		γ
M4	2.73	**M7**	8.25	**M10**	-0.03
M5	-3.67	**M8**	3.36	**M11**	0.22
M6	-1.24	**M9**	-0.30	**M12**	0.21

The full phonon dispersion curves, Figure S5.1 exhibit a significant hardening of the lattice modes across the Brillouin zone

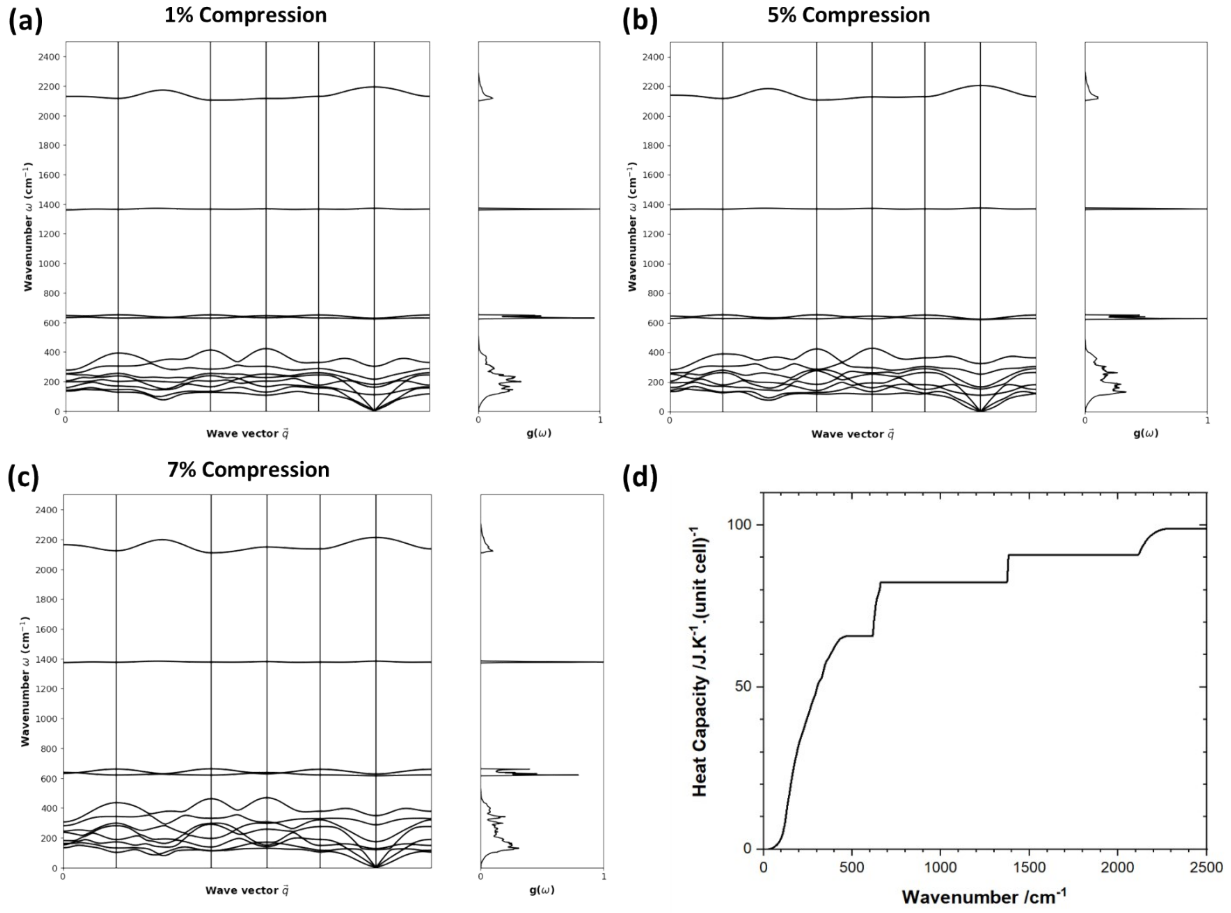

Figure S5.1 Effects of uniaxial compression of the *a* axis on the phonon dispersion of LiN_3 at (a) 1%, (b) 5%, and (c) 7% compression. (d) The vibrational heat capacity for LiN_3 at 7% compression of the *a* axis.

S5.2 Anisotropic Compression of *b* axis.

To explore uniaxial compression of the b axis, the b axis was systematically compressed while the remaining unit cell parameters and ion positions were allowed to relax, Table S5.4 To a maximum strain of *ca.* 7% on the *b* axis, the overall volume of the unit cell reduces by *ca.* 4.2% with slight expansion of the crystallographic *c* axis being observed. With compression of the *b* axis, three of the external modes harden, whereas two soften (M5 and M6), Table S5.5. these are the same modes that soften with the *a* axis is compressed (see Table S5.3). Consistent with compression of the *a* axis, the M7 mode has the larges absolute Grüneisen parameter, although somewhat smaller when the *b* axis is compressed, Table S5.6. The mode averaged Grüneisen parameter for uniaxial compression of the *b* axis is 0.75, notably smaller than achieved uniaxial compression of the *a* axis, suggesting that the mechanochemical reactivity may differ depending which face is exposed to the mechanical action.

Hardening of vibrations is observed across the Brillouin zone with uniaxial compression of the *c* axis, Figure S5.2.

Table S5.4 Effects of anisotropic compression of *b* axis on the lattice parameters.

b/b_0 /%	**a**	**b**	**c**	α	β	γ	**Vol**
1	3.245	3.210	4.934	75.783	103.549	118.351	43.433
5	3.256	3.080	4.944	76.815	103.582	117.191	42.453
7	3.269	3.016	4.961	76.923	103.528	116.889	41.995

Table S5.5 Effect of anisotropic compression of the b axis on the Γ point vibrations of LiN_3

1% Compress.				5% Compress.				7% Compress.			
	ν /cm^{-1}		ν /cm^{-1}		ν /cm^{-1}		ν /cm^{-1}		ν /cm^{-1}		ν /cm^{-1}
M4	110.05	**M9**	622.64	**M4**	110.51	**M9**	623.05	**M4**	111.13	**M9**	622.90
M5	160.35	**M10**	627.81	**M5**	154.18	**M10**	624.77	**M5**	139.89	**M10**	623.56
M6	179.19	**M11**	1371.88	**M6**	166.26	**M11**	1377.39	**M6**	168.28	**M11**	1379.85
M7	214.47	**M12**	2193.82	**M7**	252.50	**M12**	2206.60	**M7**	267.71	**M12**	2212.93
M8	301.94			**M8**	324.61			**M8**	334.82		

Table S5.6 Mode Grüneisen parameters (γ) for uniaxial compression of the *b* axis to a strain of 7%.

	γ		γ		γ
M4	1.03	**M7**	7.16	**M10**	-0.18
M5	-2.22	**M8**	2.75	**M11**	0.17
M6	-2.09	**M9**	-0.06	**M12**	0.23

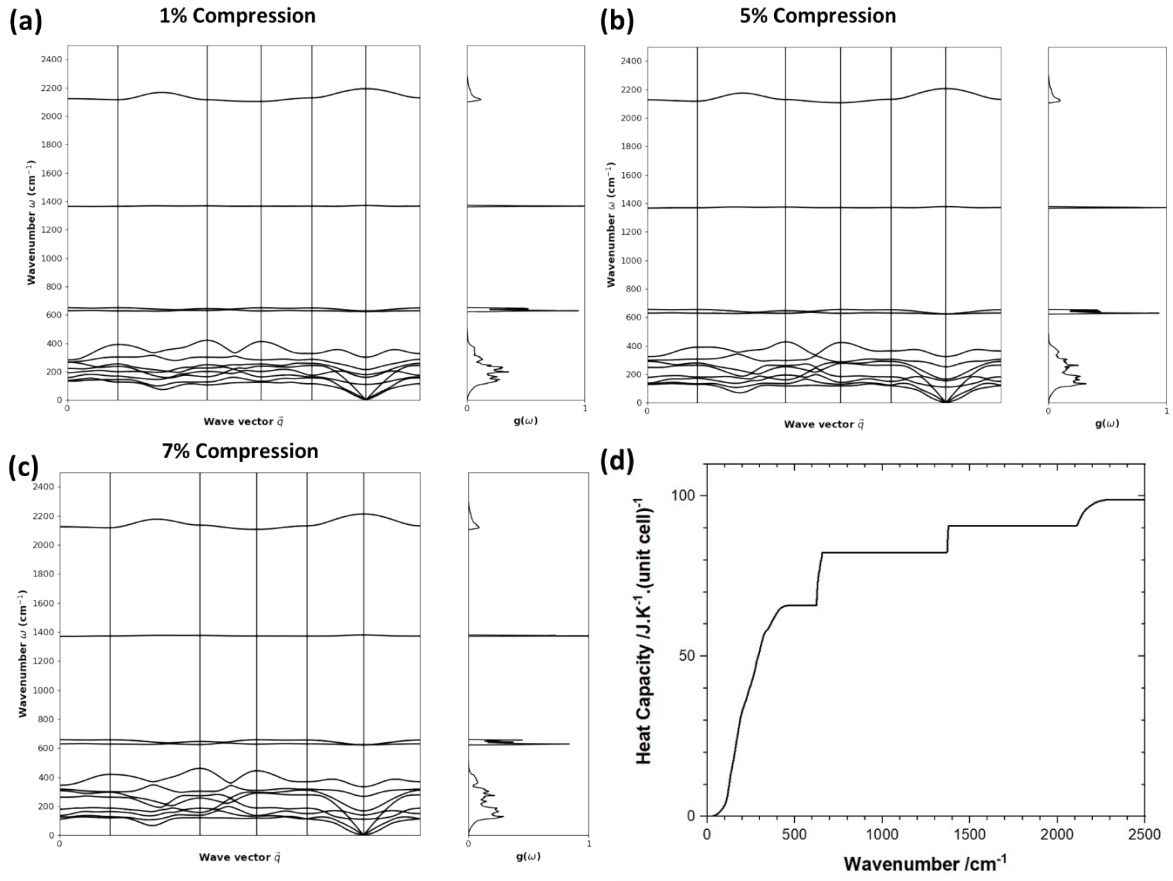

Figure S5.2 Effects of uniaxial compression of the *b* axis on the phonon dispersion of LiN_3 at (a) 1%, (b) 5%, and (c) 7% compression. (d) The vibrational heat capacity for LiN_3 at 7% compression of the *b* axis.

S5.3 Anisotropic Compression of *c* axis.

To explore uniaxial compression of the c axis, the c axis was systematically compressed while the remaining unit cell parameters and ion positions were allowed to relax, Table S5.4 To a maximum strain of *ca.* 7% on the *b* axis, the overall volume of the unit cell reduces by *ca.* 4.0%. Unlike compression of the *a* and *b* axes, compression of the *c* axis leads to hardening of *all* five external modes, Table S5.8, with negligible softening of the internal modes. Correspondingly, the average Grüneisen parameter for compression of the *c* axis, Table S5.9, is 2.59. This is significantly larger than compression along either the *a* or *b* axes, and is even larger than the average Grüneisen parameter obtained under hydrostatic compression (see Table S2.1). This provides strong evidence that mechanochemical reactivity of LiN_3 is directionally dependent, a phenomenon that will be explored in greater detail in future work.

Hardening of vibrations is observed across the Brillouin zone with uniaxial compression of the *c* axis, Figure S5.3.

Table S5.7 Effects of anisotropic compression of *c* axis on the lattice parameters.

c/c_0 /%	**a**	**b**	**c**	α	β	γ	**Vol**
1	3.239	3.239	4.905	76.443	103.557	118.284	43.596
5	3.243	3.243	4.706	78.800	101.200	117.533	42.736
7	3.235	3.235	4.607	79.701	100.299	116.801	42.069

Table S5.8 Effect of anisotropic compression of the c axis on the Γ point vibrations of LiN_3

1% Compress.				5% Compress.				7% Compress.			
	ν /cm^{-1}		ν /cm^{-1}		ν /cm^{-1}		ν /cm^{-1}		ν /cm^{-1}		ν /cm^{-1}
M4	110.26	**M9**	623.62	**M4**	122.24	**M9**	619.48	**M4**	139.64	**M9**	618.96
M5	164.64	**M10**	626.78	**M5**	199.23	**M10**	620.51	**M5**	211.81	**M10**	619.15
M6	188.41	**M11**	1370.89	**M6**	206.59	**M11**	1377.09	**M6**	217.14	**M11**	1377.30
M7	207.63	**M12**	2190.42	**M7**	212.95	**M12**	2189.89	**M7**	221.13	**M12**	2181.19
M8	304.44			**M8**	304.06			**M8**	319.67		

Table S5.9 Mode Grüneisen parameters (γ) for uniaxial compression of the *c* axis to a strain of 7%.

	γ		γ		γ
M4	7.41	**M7**	1.76	**M10**	-0.35
M5	8.90	**M8**	1.54	**M11**	0.13
M6	4.23	**M9**	-0.21	**M12**	-0.11

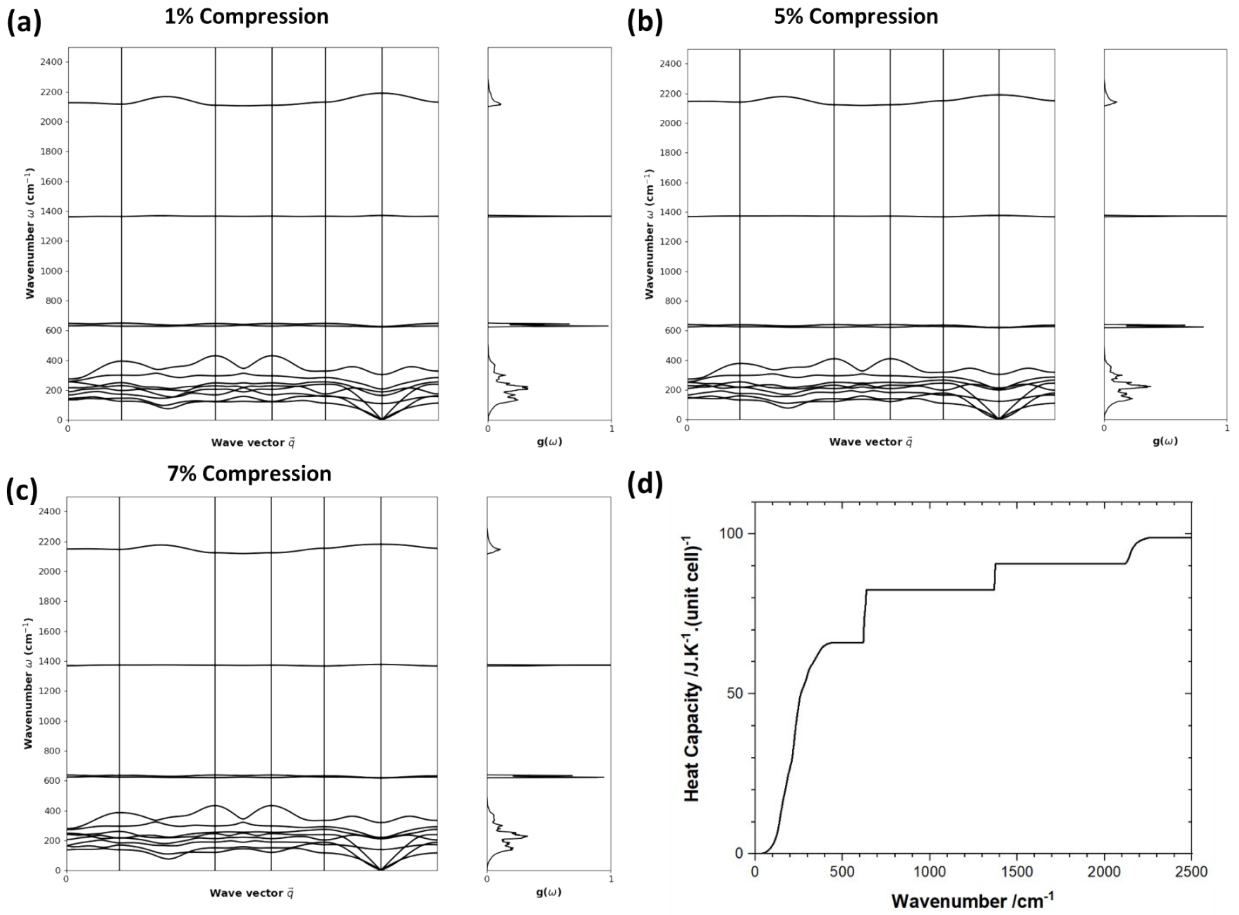

Figure S5.3 Effects of uniaxial compression of the *c* axis on the phonon dispersion of LiN_3 at (a) 1%, (b) 5%, and (c) 7% compression. (d) The vibrational heat capacity for LiN_3 at 7% compression of the *c* axis.